Shape Control of a Snake Robot with Joint Limit and Self-Collision Avoidance

Motoyasu Tanaka, *Member, IEEE,* and Kazuo Tanaka, *Fellow, IEEE*

***Abstract*—This paper proposes a shape control method for a snake robot, which maintains head position and orientation, and avoids joint limits and self-collision. We used a passive wheeled snake robot that can switch the grounded/lifted status of its wheels. We derived a kinematic model of the robot that represents its redundancy as both joint angles (the shape controllable points) and the null space of the control input. In the control method, the shape is changed by sequential control of the shape controllable points, and the null space of the control input is used for joint limit and self-collision avoidance. Jumps in control input do not occur, although the controlled variable and the model are switched. Simulations and an experiment were used to demonstrate the effectiveness of the proposed method.**

***Index Terms*—Snake robot, Shape control, Joint limit, Self-collision, Redundancy, Switching constraints, Shape controllable points.**

I. Introduction

SNAKE robots are inspired by the morphology of biological snakes. They can move by undulating their bodies like a real snake because they have a mechanism that generates anisotropic friction, making it hard to slip to sideways. Heretofore, many snake robots and associated control methods have been developed (see [1]). One type of robot developed by Hirose [2] has many active joints, passive wheels, and links serially connected by active joints. The passive wheels provide anisotropic friction to each link of the robot. This paper focuses upon snake robots with passive wheels.

When the robot continuously executes two gait patterns, the robot prepares for the next gait pattern after it finishes the preceding gait. In this case, the robot moves to an initial position and appropriately adjusts the shape of its body with respect to the next gait. These preparations are important because they improve the success rate and decrease the risk of failure. They are also required when the robot makes a repeat attempt after failure.

One of the potential applications of snake robots is investigation and search-and-rescue in narrow spaces, in and out of pipes, and at an urban disaster sites. There are occasions when the snake robot must raise its head for search and locomotion, as in [3]–[8]. The body shape of the robot needs to be appropriate for fall avoidance, because the head-raising motion increases the risk of falling. If the snake robot leaps into the air as in [9], the body needs to change to the optimal shape to prevent the wheels from slipping sideways before leaping. These previous works have not mentioned how to change the body shape to the initial shape before beginning the other gait pattern, e.g., from the motion on the flat plane to the head-raising, and from undulating to leaping into the air. If the robot change its shape while maintaining the position of its head or center of gravity, the robot can smoothly change the gait pattern, and this is the goal of the paper.

Two main models are used to control the position or trajectory of the snake robot. One considers the anisotropic friction of the body, meaning that tangential friction is low and lateral friction is high, and is used for a controller of the center of gravity (COG) in [10]–[13]. The other model, used in [6], [14]–[17], considers the nonholonomic constraint, which prevents the wheels from skidding. Head position control using the Lyapunov method in [14] or using the constraint force of wheels in [15], and trajectory tracking control of head position and orientation by introducing wheel-less links in [6], [17] have been presented.

Articulated robots, which have many joints and a slender body, including snake robots, have sensors attached to the head, e.g. vision and light-radar (lidar), for example [18]–[23]; measurement and motion planning in the robot are performed using the sensors. If the robot is tele-operated, it is relatively easy to operate the robot and to plan the motion on the basis of the head because the sensor is attached to the head. Moreover, the operator can focus the head position and orientation upon the target by checking the vision and sensor information from the head. Consequently, the robot may smoothly begin the next gait, such as head raising [3]–[6] and climbing a step as [7], [8]. Hence, rather than setting the COG this paper uses the head of the robot as the controlled point, and aims to change the body shape whilst keeping head position and orientation.

With respect to the shape control of the snake robot, singular configuration avoidance in [17], improving static stability in [6], obstacle-aided motion in [24], [25], and obstacle avoidance in [26]–[28] have been presented. These methods allow the robot to change shape while moving forward; however, the robot cannot change the body shape while maintaining the position of the head or COG. Ishikawa [16] has presented the point-to-point control of joint angles using nonlinear theory; however, the position of the head or COG cannot be controlled.

If skidding wheels are permitted, change of the body shape is easy. It is accomplished by position control of all joints at the same time or in sequence. However, it requires large torque at the joints to let the wheels skid, and position error of the head occurs. Thus, shape control with skidding wheels is undesirable from the point of view of the necessary torque and the position error.

M. Tanaka and K. Tanaka are with the Department of Mechanical and Intelligent Systems Engineering, The University of Electro-Communications, Tokyo 182-8585 Japan. (e-mail: mtanaka@uec.ac.jp).

Manuscript received Month Day, 20XX; revised Month Day, 20XX.

Next, we consider the method without skidding wheels. If all wheels touch the ground, the body shape is not freely changed because the nonholonomic constraint caused by the wheels interrupts it. In contrast, we have proposed the control method [22], [29] by which the head tracks the desired trajectory, and the body shape of the robot is freely determined at some level using the switch of allocation of the grounded/lifted parts of the body. Thus, we have proposed an approximate path-tracking controller for all joints [30]. However, it is an approximate tracking and joint limit avoidance is not considered in the method.

This paper presents a shape control method for a snake robot while maintaining the head position and orientation. A similar method has been proposed in [31] but it has two problems, one is the violation of joint limit, another is the jump of the control input. In contrast, the method proposed in this paper uses a combination of the redundant input and the switch of allocation of the grounded/lifted wheels, and avoids joint limit and self-collision. Moreover, the jump in joint input does not occur, although the controlled variable and the model are switched.

The contributions of the paper are as follows:

- The proposed method enables a snake robot to appropriately adjust its body shape in the intervening period between two gait patterns. In particular, the actual robot must avoid violation of joint limits and self-collision.
- The model in which the redundancy of the system is represented as both joint angles (called the shape controllable points) and null space is derived. Their combination makes the control method more varied. Shape control is one of the usage examples of the model.
- The joint input without jumps is presented; however, the controlled variable and the model are switched.
- The proposed method is easy to apply for an articulated mobile robot which has active wheels and many links serially connected by active joints as [34]–[39] if the robot can switch the grounded/lifted status of wheels. This is because the model and controller in the proposed method is based on the nonholonomic constraint of wheels, and they are similar to those of the articulated mobile robot presented in [34].

The rest of the paper is organized as follows: In section II, the kinematic model of the snake robot is derived and the joint input is provided as the basis for the shape control method. Section III presents the outline of the shape control method, introducing phase, and suppressing input jumps depending on the switch of the controlled variable. Section IV presents the method for avoiding joint limit and self-collision. Section V and VI provides a demonstration of effectiveness of the proposed method by simulations and an experiment.

II. Model and joint input

We use an $n+1$-link snake robot as shown in Fig.1. A link comprises a pitch rotational joint and a pair of wheels, and is connected to an adjoining link via a yaw rotational joint. The passive wheel is coaxially placed at the pitch joint, except for the first link. All joints are active and all wheels are passive.

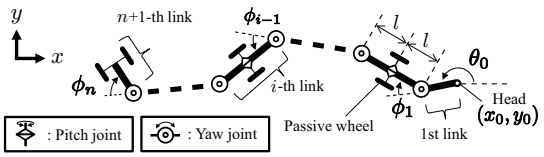

Fig. 1. Model of a snake robot.

A. Model

Let $\boldsymbol{w} = [x_0, y_0, \theta_0]^{\mathrm{T}}$ be the position and orientation of the robot's head, ϕ_i be the joint angle of the i-th yaw joint, let us define $\boldsymbol{\phi} = [\phi_1, \cdots, \phi_n]^{\mathrm{T}}$ and $\boldsymbol{q} = [\boldsymbol{w}^{\mathrm{T}}, \boldsymbol{\phi}^{\mathrm{T}}]^{\mathrm{T}}$. Assuming that the passive wheel does not slide in a sideways direction, the velocity constraints are expressed as

$$\boldsymbol{A}\dot{\boldsymbol{w}} = \boldsymbol{B}\boldsymbol{u}, \tag{1}$$

where $\boldsymbol{u} = \dot{\boldsymbol{\phi}}$, $\boldsymbol{A} \in \mathbb{R}^{n\times 3}$, and $\boldsymbol{B} \in \mathbb{R}^{n\times n}$. The $1, \cdots, n$-th row of $\boldsymbol{A}$ and $\boldsymbol{B}$ correspond to the velocity constraint of $1, \cdots, n$-th wheel, respectively. Next, we introduce the lifted wheel which does not touch the ground into the system (1). Note that wheels can be lifted by slightly rotating the pitch joints [22], [29]–[31]. Then, the velocity constraints of the wheels are different depending on the grounded/lifted status of wheels. We allocate a unique integer σ, called the *mode*, to represent the overall status of the wheels [29]. If $n'_1, \cdots, n'_{\bar{n}_\sigma}$-th wheels (the total number is $\bar{n}_\sigma$) don't touch the ground in the mode σ, the velocity constraints are expressed as

$$\bar{\boldsymbol{A}}_\sigma \dot{\boldsymbol{w}} = \bar{\boldsymbol{B}}_\sigma \boldsymbol{u}, \tag{2}$$

where $\bar{\boldsymbol{A}}_\sigma \in \mathbb{R}^{(n-\bar{n}_\sigma)\times 3}$ and $\bar{\boldsymbol{B}}_\sigma \in \mathbb{R}^{(n-\bar{n}_\sigma)\times n}$ are the matrices whose $n'_1, \cdots, n'_{\bar{n}_\sigma}$-th row vectors are eliminated from the matrices $\boldsymbol{A}$ and $\boldsymbol{B}$, respectively. The aforementioned formulation follows previous work [29]. The system (2) has kinematic redundancy. The degree of redundancy is $n - (n - \bar{n}_\sigma) = \bar{n}_\sigma$ because it is the difference between the number of rows and the number of columns of $\bar{\boldsymbol{B}}_\sigma$. In this paper, we add the shape controllable points (SCPs) [6], [17] into the controlled variables to represent the subset of kinematic redundancy. The SCP is the joint angle of the link which has the lifted wheel, and can be directly controlled because it is contained in the controlled variables. Let m be the number of SCPs where $m \leq \bar{n}_\sigma$, the $\tilde{n}_1, \cdots, \tilde{n}_m$-th yaw joint be the SCP, $\tilde{\boldsymbol{\phi}}_\sigma = [\phi_{\tilde{n}_1}, \cdots, \phi_{\tilde{n}_m}] \in \mathbb{R}^m$ is the joint angle of SCPs, $\tilde{\boldsymbol{w}}_\sigma = [\boldsymbol{w}^{\mathrm{T}}, \tilde{\boldsymbol{\phi}}_\sigma^{\mathrm{T}}]^{\mathrm{T}}$ is the controlled variable including the SCP, and ΔT is the switching period for the mode. The kinematic model of the robot with switching modes is expressed as

$$\tilde{\boldsymbol{A}}_{\sigma(t)} \dot{\tilde{\boldsymbol{w}}}_{\sigma(t)} = \tilde{\boldsymbol{B}}_{\sigma(t)} \boldsymbol{u}, \tag{3}$$

$$\sigma(t) = \sigma_k, \quad (t_k \leq t < t_{k+1}) \tag{4}$$

where $\sigma \in \{1, 2, \cdots, N_{\mathrm{m}}\}$, N_{m} is the number of modes, $t_k = k\Delta T$ $(k = 0, 1, \cdots)$ is the switching time of the mode,

$$\tilde{\boldsymbol{A}}_\sigma = \begin{bmatrix} \bar{\boldsymbol{A}}_\sigma & \boldsymbol{0} \\ \boldsymbol{0} & \boldsymbol{I}_m \end{bmatrix} \in \mathbb{R}^{(n-\bar{n}_\sigma+m)\times(3+m)}, \tag{5}$$

$$\tilde{\boldsymbol{B}}_\sigma = \begin{bmatrix} \bar{\boldsymbol{B}}_\sigma \\ \boldsymbol{C}_\sigma \end{bmatrix} \in \mathbb{R}^{(n-\bar{n}_\sigma+m)\times n}, \tag{6}$$

and $\boldsymbol{C}_\sigma \in \mathbb{R}^{m\times n}$. Let $c_{\{i,j\}}$ be the i-th row j-th column element of $\boldsymbol{C}_\sigma$. In $\boldsymbol{C}_\sigma$, $c_{\{1,\tilde{n}_1\}} = c_{\{2,\tilde{n}_2\}} = \cdots = c_{\{m,\tilde{n}_m\}} = 1$ and the other elements are zero.

(3) is a hybrid system switching models every ΔT. The mode is maintained during ΔT, and is switched every ΔT. This paper use (3) as the kinematic model of the snake robot.

If only $\tilde{n}_1, \cdots, \tilde{n}_m$-th wheel is lifted and the other wheels touch the ground, the kinematic model is obtained as

$$\tilde{\boldsymbol{A}}_\sigma^{'} \dot{\tilde{\boldsymbol{w}}}_\sigma = \tilde{\boldsymbol{B}}_\sigma^{'} \boldsymbol{u}, \tag{7}$$

where

$$\tilde{\boldsymbol{A}}_\sigma^{'} = \begin{bmatrix} \bar{\boldsymbol{A}}_\sigma^{'} & \boldsymbol{0} \\ \boldsymbol{0} & \boldsymbol{I}_m \end{bmatrix} \in \mathbb{R}^{n\times(3+m)}, \ \tilde{\boldsymbol{B}}_\sigma^{'} = \begin{bmatrix} \bar{\boldsymbol{B}}_\sigma^{'} \\ \boldsymbol{C}_\sigma \end{bmatrix} \in \mathbb{R}^{n\times n},$$

and $\bar{\boldsymbol{A}}_\sigma^{'}$ and $\bar{\boldsymbol{B}}_\sigma^{'}$ are the matrices whose $\tilde{n}_1, \cdots, \tilde{n}_m$-th row vectors are eliminated from the matrices $\boldsymbol{A}$ and $\boldsymbol{B}$, respectively. $\tilde{\boldsymbol{A}}_\sigma$ and $\tilde{\boldsymbol{B}}_\sigma$ are the matrices in which some rows are eliminated from $\tilde{\boldsymbol{A}}_\sigma^{'}$ and $\tilde{\boldsymbol{B}}_\sigma^{'}$, respectively. Thus, $\tilde{\boldsymbol{A}}_\sigma$ and $\tilde{\boldsymbol{B}}_\sigma$ can be represented as

$$\tilde{\boldsymbol{A}}_\sigma = \boldsymbol{T}_\sigma \tilde{\boldsymbol{A}}_\sigma^{'}, \ \tilde{\boldsymbol{B}}_\sigma = \boldsymbol{T}_\sigma \tilde{\boldsymbol{B}}_\sigma^{'}, \tag{8}$$

where $\boldsymbol{T}_\sigma \in \mathbb{R}^{(n-\bar{n}_\sigma+m)\times n}$ is a selection matrix for which the elements are either 0 or 1.

B. Joint input without jumps

We have proposed a controller which connects the joint input without jumps for an articulated mobile robot with switching modes [34]. This paper also designs a joint input $\boldsymbol{u}$ as follows.

$$\boldsymbol{u} = \boldsymbol{u}_{\sigma\mathrm{t}} + \boldsymbol{u}_{\sigma\mathrm{ker}}, \tag{9}$$

$$\boldsymbol{u}_{\sigma\mathrm{t}} = \tilde{\boldsymbol{B}}_\sigma^{'-1} \tilde{\boldsymbol{A}}_\sigma^{'} \{\dot{\tilde{\boldsymbol{w}}}_{\sigma\mathrm{d}} - \boldsymbol{K}_\sigma(\tilde{\boldsymbol{w}}_\sigma - \tilde{\boldsymbol{w}}_{\sigma\mathrm{d}})\}, \tag{10}$$

$$\boldsymbol{u}_{\sigma\mathrm{ker}} = -k_\eta (\boldsymbol{I} - \tilde{\boldsymbol{B}}_\sigma^{\dagger} \tilde{\boldsymbol{B}}_\sigma)\boldsymbol{\eta}, \tag{11}$$

where $\boldsymbol{K}_\sigma > \boldsymbol{0}$ is the matrix of the feedback gain, $\tilde{\boldsymbol{w}}_{\sigma\mathrm{d}}$ is the desired value of $\tilde{\boldsymbol{w}}_\sigma$, $k_\eta \geq 0$ is the gain related to redundancy, $\tilde{\boldsymbol{B}}_\sigma^{\dagger}$ is the pseudo inverse matrix of $\tilde{\boldsymbol{B}}_\sigma$, $\boldsymbol{\eta} \in \mathbb{R}^n$ is an arbitrary vector related to the redundancy. $\boldsymbol{u}_{\sigma\mathrm{t}}$ is the element related to tracking of the controlled variable and $\boldsymbol{u}_{\sigma\mathrm{ker}}$ is the element related to redundancy.

By substituting (8) and (9) into (3), the closed-loop system is obtained as

$$\tilde{\boldsymbol{A}}_\sigma \left(\dot{\boldsymbol{e}}_\sigma + \boldsymbol{K}_\sigma \boldsymbol{e}_\sigma\right) = \boldsymbol{0}, \tag{12}$$

where $\boldsymbol{e}_\sigma = \tilde{\boldsymbol{w}}_\sigma - \tilde{\boldsymbol{w}}_{\sigma\mathrm{d}}$. If $\tilde{\boldsymbol{A}}_\sigma$ is full column rank, (12) has a unique solution as follows.

$$\dot{\boldsymbol{e}}_\sigma + \boldsymbol{K}_\sigma \boldsymbol{e}_\sigma = \boldsymbol{0}. \tag{13}$$

From (13), $\tilde{\boldsymbol{w}}_\sigma$ converges to $\tilde{\boldsymbol{w}}_{\sigma\mathrm{d}}$ at $t \to \infty$. Note that $\tilde{\boldsymbol{w}}_\sigma$ includes the SCPs in the mode σ. The rank deficiency of $\tilde{\boldsymbol{A}}_\sigma$ represents the singular configuration of the robot, which it has to avoid.

If $m = \bar{n}_\sigma$, $\boldsymbol{u}_{\sigma\mathrm{ker}}$ disappears because $\tilde{\boldsymbol{B}}_\sigma \in \mathbb{R}^{n\times n}$ is invertible. This means that all degrees of redundancy are represented as the SCP and the rest of the degree of redundancy is zero. In contrast, if $m < \bar{n}_\sigma$, $\boldsymbol{u}_{\sigma\mathrm{ker}}$ exists and it means that the rest of the degree of redundancy exists.

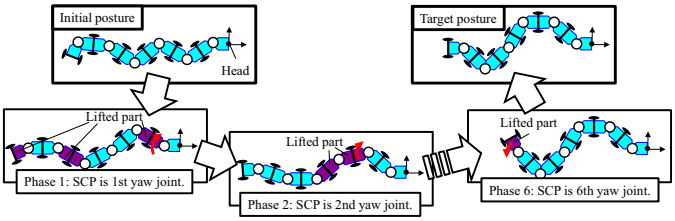

Fig. 2. Outline of shape control method if $n = 6$.

C. Redundant input without jumps

In [6], [17], all degrees of redundancy are represented as the SCPs and then $m = \bar{n}_\sigma$. In this paper, the degree of redundancy is retained by setting $m \leq \bar{n}_\sigma$, and both the SCPs and remaining degree of redundancy are used in parallel. We define the control objective as follows. The main control objective is to maintain the head position and orientation, and to change the body shape of the robot. Shape control is partially obtained by controlling the angle of SCPs. The sub-control objective is avoidance of joint limit, self-collision, and singular configuration, and is obtained by using the remaining degrees of redundancy.

We set the cost function $V(\boldsymbol{q})$ with respect to the sub-control objective, and aim at achieving the success of the sub-control objective by decreasing V. $\boldsymbol{\eta}$ in (11) is designed as

$$\boldsymbol{\eta} = \left[\frac{\partial V}{\partial \phi_1}, \cdots, \frac{\partial V}{\partial \phi_n}, \right]^{\mathrm{T}} \in \mathbb{R}^n. \tag{14}$$

By considering (9), the time derivative of V is

$$\frac{\mathrm{d}V}{\mathrm{d}t} = \frac{\partial V}{\partial \boldsymbol{w}} \dot{\boldsymbol{w}} + \frac{\partial V}{\partial \boldsymbol{\phi}} \boldsymbol{u}_{\sigma\mathrm{t}} - k_\eta \boldsymbol{\eta}^{\mathrm{T}} (\boldsymbol{I} - \tilde{\boldsymbol{B}}_\sigma^{\dagger} \tilde{\boldsymbol{B}}_\sigma)\boldsymbol{\eta}. \tag{15}$$

The third term of the right side of (15) contributes to the decrease of V because $(\boldsymbol{I} - \tilde{\boldsymbol{B}}_\sigma^{\dagger} \tilde{\boldsymbol{B}}_\sigma) \geq \boldsymbol{0}$ and $k_\eta \geq 0$. This means that it contributes to the accomplishment of the sub-control objective.

k_η in (11) is designed as

$$k_\eta = \{1 - \cos(2\pi t/\Delta T)\}\, k_\eta^{'}. \tag{16}$$

where $k_\eta^{'} > 0$. k_η is zero at the switching time of modes $t = t_k$ $(k = 0, 1, \cdots)$. Thus, $\boldsymbol{u}_{\sigma\mathrm{ker}}$ is connected without jumps because $\boldsymbol{u}_{\sigma\mathrm{ker}}$ is $\boldsymbol{0}$ at the switching time in all modes.

From (7) and (10), if the SCPs are equivalent in all modes, $\boldsymbol{u}_{\sigma\mathrm{t}}$ are equivalent without depending upon the mode. As a result, if the SCPs are equivalent in all modes, the joint input $\boldsymbol{u}$ does not jump despite the mode being switched.

III. Shape Control Method

We assume that the target shape is static without joint velocities and the desired value of $\boldsymbol{w}$ is constant. We directly control the SCP included in $\tilde{\boldsymbol{w}}$ to control the shape of the robot. If the joint angle of SCP changes, the joint angles at the rear of the SCP change as [6]. Thus, the shape of the body can be changed by directly controlling the SCP and sequentially switching the lifted wheels and the SCP from head to tail. Fig. 2 shows the outline of the method. First, the robot lifts

the wheels in the second link and puts ϕ_1 in $\tilde{\boldsymbol{w}}$ as the SCP. The SCP is controlled by the input (9). If the SCP converges to the desired value, the robot lets the wheels in the second link touch the ground, lifts the wheels in the third link, puts ϕ_2 in $\tilde{\boldsymbol{w}}$ as the SCP, and the SCP converges to the desired value by (9). These are sequentially modified until the wheels in the tail link are reached. In this method, the input is calculated based on the velocity constraints (3) not to let the wheels skid. Therefore, the robot does not require large torque at the joints to let the wheels skid, and the position error of the robot's head should be decreased as compared with the case where the robot changes the shape without considering the velocity constraints of wheels. If we first set the joint angle ϕ_i of the neighborhood of the tail as the SCP, the angle converges to the target once at least. However, the angle changes depending on the motion of $\phi_1, \cdots, \phi_{i-1}$ when they are the SCP. Therefore, the strategy setting SCPs out of order is inefficient as compared with the proposed strategy.

In [31], all wheels except the wheel corresponding to the SCP touch the ground. By contrast, in this paper, some wheels except the wheel corresponding to the SCP are lifted as can be seen in Fig. 2, and the robot accomplishes the sub-control objective: avoidance of joint limit, self-collision, and singular configuration. Here, we define that all forward wheels of the SCP touch the ground because the shape control in the forward links of the SCP is completed. Thus, we can design the grounded/lifted status of only the rearward wheels of the SCP.

A. Phase shift

We define the case where the SCP is ϕ_i as the *phase* i. The candidates for allocation of the grounded/lifted wheels are different with respect to each phase. This is trivial because the wheel corresponding to the SCP is always lifted and all forward wheels of the SCP always touch the ground. Thus, we define the relationship between the mode number σ and the allocation of the grounded/lifted wheels with respect to each phase.

The controlled variable is different with respect to each phase because of the difference of the SCP. If phase is i, then the controlled variable is $\tilde{\boldsymbol{w}}_\sigma = [\boldsymbol{w}^{\mathrm{T}}, \phi_i]^{\mathrm{T}}$. Since the target shape is static without joint velocities, the desired velocity of the controlled variable is

$$\dot{\tilde{\boldsymbol{w}}}_{\sigma \mathrm{d}} = [0, 0, 0, 0]^{\mathrm{T}}. \tag{17}$$

If the SCP ϕ_i converges to the desired value $\phi_{i\mathrm{d}}$, then the phase shifts from i to $i+1$. In the phase i, the following inequality is used for the convergence test at the switching time of modes $t = t_k$.

$$|\phi_i - \phi_{i\mathrm{d}}| < \epsilon_{\mathrm{p}}, \tag{18}$$

where $\epsilon_{\mathrm{p}} > 0$ is a small constant.

B. Input smoothing

We propose a smoothing method for the joint input without jumps where the mode and phase are switched. In each phase, the SCP is not switched in all modes. From section II-B and II-C, the joint input is connected without jumps in each phase though the mode is switched. However, the joint angle corresponding to the SCP is replaced when the phase is shifted. Then, $\boldsymbol{u}_{\sigma \mathrm{t}}$ in the joint input jumps because the SCP in the controlled variable is replaced.

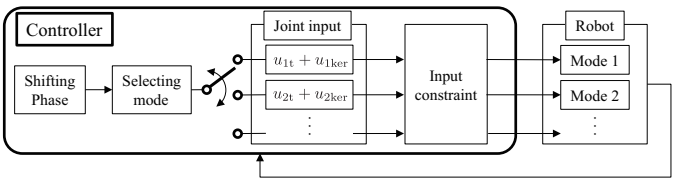

Fig. 3. Control diagram of the proposed method.

Assuming that the error of $\boldsymbol{w}$ is very small, we consider the shift of phase from i to $i+1$. When the phase i finishes, $\boldsymbol{u}_{\sigma \mathrm{t}} \simeq 0$ because of (18). Thus, we design that $\boldsymbol{u}_{\sigma \mathrm{t}}$ smoothly increases from zero during the shift of phase from i to $i+1$, to connect the input without jumps. Let ϕ'_{i+1} be the ϕ_{i+1} at the time shift of the phase. In this paper, we smoothly change $\phi_{(i+1)\mathrm{d}}$ from ϕ'_{i+1} to the target value using a cam curve. Thus, $\boldsymbol{u}_{\sigma \mathrm{t}}$ is connected without jumps. As a result, the joint input is connected without jumps in spite of the mode switching and phase shifting.

IV. Avoiding Joint Limit and Self-collision

If the previous method shown in Fig. 2 is used, the joint limit violations frequently occur because the rear joints of the SCP rotate significantly. Moreover, the self-collision between the links also occurs because the snake robot has many serially connected links. In this section, we present a method by which the robot avoids the joint limit and possibly avoids the self-collision and the singular configuration. In particular, the joint limit is avoided as follows:

- Redundant input (11) is used for separating joint limit, self-collision, and singular configuration.
- The mode in which the joint limit violation will occur is not selected.
- Tracking control of the control variable is weakened depending on the margin related to the joint limit.

Fig. 3 depicts the block diagram of the proposed method including the shift of phase in the section III. Section IV-A, IV-B, IV-C, and IV-D correspond to $\boldsymbol{u}_{\sigma \mathrm{ker}}$, 'Selecting mode,' $\boldsymbol{u}_{\sigma \mathrm{t}}$, and 'Input constraint' in Fig. 3, respectively.

A. Use of redundant input

$\boldsymbol{u}_{\sigma \mathrm{ker}}$ in (9) does not affect the response of the controlled variable; it is used for the sub-control objective. Let n' be the phase number. If $n' = n$, the tail wheel is only lifted and $\boldsymbol{u}_{\sigma \mathrm{ker}} = \emptyset$. Thus, we consider the case of $n' < n$.

We define $d_{\{i,j\}}$ as $d_{\{i,j\}} = \sqrt{(x_i - x_j)^2 + (y_i - y_j)^2}$ where (x_0, y_0) is the position of the head, (x_n, y_n) is the position of the tail, and (x_i, y_i) is the position of the center of $i+1$-th link if $1 \leq i < n$. Then, the cost function V is designed as

$$V(\boldsymbol{q}) = a_{\mathrm{L}} V_{\mathrm{L}} + a_{\mathrm{c}} V_{\mathrm{c}} + a_{\mathrm{s}} V_{\mathrm{s}}, \tag{19}$$

where $V_{\rm L} = \sum_{i=n'+1}^{n} f(c_\phi, |\phi_i|)$, $V_{\rm s} = 1/\det \tilde{\boldsymbol{A}}_\sigma^{\rm T} \tilde{\boldsymbol{A}}_\sigma$, $V_{\rm c} = \sum_{i=n'+1}^{n} \sum_{j=1}^{i-3} f(d_{\{i,j\}}, d_0)$, and $a_{\rm L}, a_{\rm c}, a_{\rm s}$ are the weight constant, c_ϕ and d_0 are the activation constants for $V_{\rm L}$ and $V_{\rm c}$, respectively, and

$$f(x,y) = \begin{cases} (y-x)^3 & (\text{if} \quad x < y) \\ 0 & (\text{otherwise}) \end{cases}. \tag{20}$$

$V_{\rm L}$ and $V_{\rm c}$ are related to joint limit and self-collision, respectively, and they are the cubic function as [32], [33]. If $\tilde{\boldsymbol{A}}_\sigma$ is rank deficient, $\det \tilde{\boldsymbol{A}}_\sigma^{\rm T} \tilde{\boldsymbol{A}}_\sigma = 0$. Thus, $V_{\rm s}$ is related to the singular configuration [22], [29] and increases if the robot approaches the singular configuration. As a result, redundant input (11) avoids the joint limit, self-collision, and singular configuration by decreasing V.

B. Selecting mode

From (11), the redundant input depends on the mode σ. Moreover, the effect of the redundant input for the sub-control objective is different with respect to σ because of (15). We approach the sub-control objective using the optimal σ by switching the modes. We introduce the optimal problem as follows:

$$\min_{\sigma_k} \quad J, \tag{21}$$

$$s.t. \quad \text{Statically stable in } t_k \le t \le t_{k+1}, \tag{22}$$

$$|\phi_i(t)| \le \phi_{\rm limit} \text{ in } t_k \le t \le t_{k+1}, \tag{23}$$

where

$$J = a_{\rm scp} V_{\rm scp}(\hat{\boldsymbol{q}}(t_{k+1}, \sigma_k)) + \int_{t_k}^{t_{k+1}} V(\hat{\boldsymbol{q}}(\tau, \sigma_k)) {\rm d}\tau, \tag{24}$$

$$V_{\rm scp} = \frac{1}{|\hat{\phi}_{n'}(t_{k+1}) - \phi_{n'}(t_k)|}, \tag{25}$$

and $a_{\rm scp}$ is a weight constant. $\hat{\boldsymbol{q}}$ and $\hat{\phi}_{n'}$ are the estimated values of $\boldsymbol{q}$ and $\phi_{n'}$, respectively, and they are calculated by numerical integration of (9) and (13). $V_{\rm scp}$ is related to deadlock avoidance, and increases if the rotation amount of the SCP is small. If $a_{\rm scp} = 0$, deadlock may occur because the tracking motion of the SCP is not considered at the time selecting modes. (22) means that the robot remains statically stable. The robot is statically stable when the center of gravity of the robot exists in the support polygon constructed by the grounded points [22], [29], [40]. (23) means that the joint angles do not violate the joint limit. The solution σ_k is obtained by numerically solving (21) by comparing J calculated for all modes, and σ_k is used at $t_k \le t < t_{k+1}$.

C. Stop tracking of $\tilde{\boldsymbol{w}}_\sigma$

If the joint angle reaches the limitation angle, the robot should place a high priority upon joint limit avoidance. $\boldsymbol{u}_{\sigma{\rm t}}$ may interrupt joint limit avoidance because of (15). Thus, if the robot is in such a configuration, we stop tracking of the controlled variable $\tilde{\boldsymbol{w}}_\sigma$ by setting as $\boldsymbol{u}_{\sigma{\rm t}} = \boldsymbol{0}$. Let Φ be the minimum margin related to the joint limit in the rear joints of the SCP, and it is defined as

$$\Phi = \min\left(\phi_{\rm limit} - |\phi_i|\right), \quad i = n'+1, \cdots, n. \tag{26}$$

TABLE I
PARAMETERS OF THE SIMULATION.

n	8	$a_{\rm L}$	2.1	k_0	$\pi/4$ [rad]
l	0.091 [m]	$a_{\rm c}$	6.7×10^2	k'_η	2
ΔT	3 [s]	$a_{\rm s}$	2×10^{-3}	$\boldsymbol{K}'_\sigma$	diag(1, 1, 0.5, 2)
c_ϕ	$\pi/4$ [rad]	$a_{\rm scp}$	1×10^{-4}	$\phi_{\rm limit}$	$\pi/2$ [rad]
d_0	0.27[m]	$\boldsymbol{w}_d$	$[0, 0, \pi]^{\rm T}$	$u_{\rm limit}$	$\pi/4$ [rad/s]

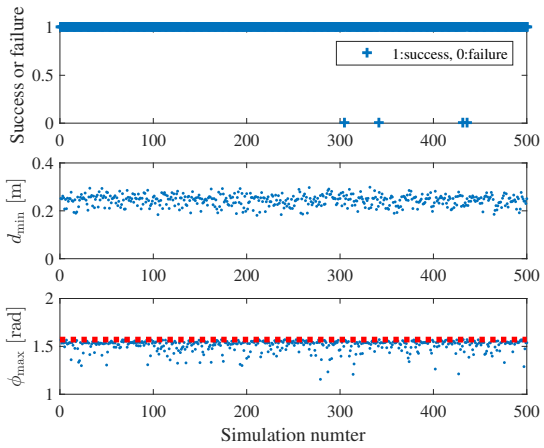

Fig. 4. Simulation results where initial and target shapes are randomly set.

We design the gain $\boldsymbol{K}_\sigma$ in (10) as

$$\boldsymbol{K}_\sigma = k_{\rm t}(\Phi) \boldsymbol{K}'_\sigma \tag{27}$$

$$k_{\rm t}(\Phi) = \begin{cases} \frac{1}{2}(1 - \cos(\frac{\pi}{k_0}\Phi)), & (\text{if} \quad \Phi < k_0) \\ 1, & (\text{otherwise}) \end{cases} \tag{28}$$

where $\boldsymbol{K}'_\sigma > \boldsymbol{0}$, and k_0 is an activation angle to stop tracking. If $k_{\rm t} = 0$, $\boldsymbol{u}_{\sigma{\rm t}} = \boldsymbol{0}$ from (10) and (17). By design the gain as described in (27) and (28), the effect of tracking control is weakened at $\Phi < k_0$, and becomes zero at $\Phi = 0$ because of $k_{\rm t} = 0$.

D. Input constraint

By considering the experiment using a real robot, we set the input constraint. Let $u_{\rm limit}$ be the limit value of the absolute angular velocity of the joint, and $\max|\dot{\phi}_i|$ be the maximum value of $|\dot{\phi}_i|$. If $\max|\dot{\phi}_i| > u_{\rm limit}$, the input should be decreased. Thus, we adjust the input (9) as

$$\boldsymbol{u} = k_u(\boldsymbol{u}_{\sigma{\rm t}} + \boldsymbol{u}_{\sigma{\rm ker}}), \tag{29}$$

$$k_u = \begin{cases} \frac{u_{\rm limit}}{\max|\dot{\phi}_i|}, & \text{if} \quad u_{\rm limit} < \max|\dot{\phi}_i| \\ 1, & \text{otherwise} \end{cases}. \tag{30}$$

As a result, the input is constrained in the limit value without breaking the kinematic relationship. Note that the convergence of the controlled variable becomes slow and the contribution for the sub-control objective decreases as compared with the case using (9) without input constraint.

V. SIMULATION

Table I shows the parameters of the simulations; the initial state of $\boldsymbol{w}$ and its desired state $\boldsymbol{w}_d$ are $[0, 0, \pi]^{\mathrm{T}}$. The sampling time was 0.02 [s]. The 500 simulations were carried out randomly by setting the initial and target shapes. Then, we eliminated the initial and target shape in which self-collision occurs. Let $\phi_{\max}$ be the maximum absolute angle of the joints, and $d_{\min}$ be the minimum distance between the center position of the links which have the possibility of self-collision. We set the case where the robot converges upon the target shape as a success, and the case where the robot does not converge to it by deadlock as a failure.

The simulation results using the proposed method are depicted in Fig. 4. The 496 patterns were a success with a success rate of 99.2%. The minimum value of $d_{\min}$ is 0.18 [m]. The minimum elapsed time from start to finish is 27 [s], and the maximum time is 180 [s] excepting the failure cases. The deadlock depends on static stability of (22) and interference between the cost functions in (24). We tuned parameters rising the success rate with preventing the interference through trial and error considering balance of $a_{\mathrm{L}}V_{\mathrm{L}}$ and $a_{\mathrm{c}}V_{\mathrm{c}}$ as table I. Note that the success rate drops depending on the parameters. We found that the joint limit and self-collision avoidance were satisfied from Fig. 4.

Let $\boldsymbol{\phi}(0)$ be the initial angle of $\boldsymbol{\phi}$, and $\boldsymbol{\phi}_{\mathrm{d}}$ be the target angle. Fig. 5 depicts the result of simulation number 1 where $\phi(0) = [0.63,\ -0.44,\ -1.57,\ -0.36,\ -0.57,\ -0.34,\ -1.00,\ -0.91]^{\mathrm{T}}$ and $\phi_{\mathrm{d}} = [0.29,\ 0.30,\ -1.02,\ 1.36,\ -1.39,\ -0.94,\ 0.025,\ 0.81]^{\mathrm{T}}$, as an example of success pattern. From Fig. 5 (a), the head position and orientation maintained the desired value, and the joint angles finally converged to the target angle without violating the joint limit. We found that the joint input did not jump in spite of the mode switch and the phase shift from Fig. 5 (b). Thus, the effectiveness of the proposed method was demonstrated.

VI. EXPERIMENT

We used the snake robot shown in Fig. 6 where n and l are equivalent to the simulations. The actuator was a smart actuator module (Dynamixel MX-106, ROBOTIS). The head motion was measured by the motion capture system (Opti-Track, NaturalPoint, Inc.) and the joint angles were measured by the internal encoder of the smart actuator module. The robot switches its mode slightly by rotating the pitch joints [29]. We set the mode candidates with respect to each phase as Table II. The number of modes are heuristically reduced because of the calculation time of (21) in the experiment using a real robot. The calculation amount of (21) is proportional to the number of modes because $\hat{\boldsymbol{q}}$ and J in all modes are calculated in the optimal problem. In the phase 1, the maximum number of modes is 99. By decreasing the number from 99 to 14, the calculation time decreases by about 85% . The mode candidates are empirically selected considering both the torque limit of the pitch joint and deadlock avoidance. Considering the calculation time of mode selection, we set that the sampling time as 0.2 [s] and decreased the gain compared with simulations $a_{\mathrm{c}} = 67$, $\boldsymbol{K}'_{\sigma} = \mathrm{diag}(1, 1, 0.5, 0.5)$, and

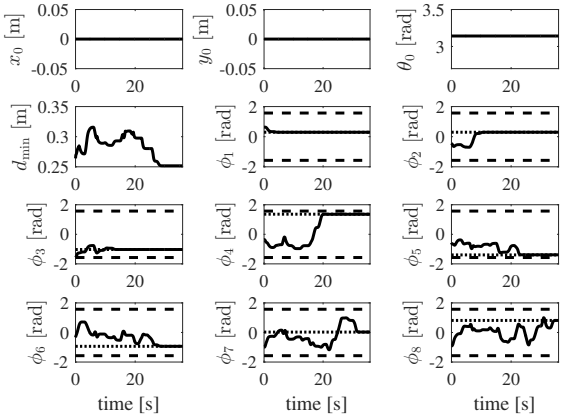

(a) x_0, y_0, θ_0, $d_{\min}$, $\boldsymbol{\phi}$.

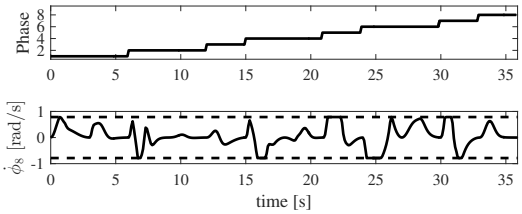

(b) Phase and an element of $\boldsymbol{u}$ ($\dot{\phi}_8$).

Fig. 5. Time responses in the simulation number 1. The broken line is the limit, and the dotted line is the target value.

$k'_{\eta} = 1$. The controller was implemented on the PC (intel Core i7-3930K CPU, 16GB RAM, and Windows 7) using MATLAB 2014a with parallel computing toolbox. The optimal problem (21) was solved using parallel computing, and the maximum time for solving it is 0.15 [s] in the phase 1. The maximum time of the control loop is 0.18 [s]. The initial and target shapes were equivalent to simulation number 1.

Fig. 7 (a) depicts the result where all joints changed to the target angle at the speed $\pi/4$ [rad/s]. In this case, large error of the head position and orientation occurred and the error of x_0, y_0, θ_0 were 0.07[m], 0.38[m], and 1.1[rad], respectively.

Figs. 7 (b) and 8 depict the result using the proposed method. The robot changed the body shape from head to tail as Fig. 7 (b). $\boldsymbol{w}$ converged to the desired value $[0, 0, \pi]^{\mathrm{T}}$ and joint angles did not violate the limit as Fig. 8. However, the error of the body shape finally occurred as shown by the the joint angles in Fig. 8. The maximum error was 0.18 [rad] in ϕ_3. This was caused by the motion for tracking of $\boldsymbol{w}$ when the error of $\boldsymbol{w}$ occurred after the control of ϕ_3 as the SCP finished. We suspect that the error of $\boldsymbol{w}$ was caused by the lateral slip of the wheels and the motion of the pitch joints for lifting the wheels.

As a result, we confirmed that the proposed method accomplished the shape control whilst maintaining head position and avoiding joint limit and self-collision. The error of the joint

TABLE II
MODE AND WHEEL STATUS.

Phase	Mode num.	Wheel num. (L: lifted, G: grounded) 1	2	3	4	5	6	7	8
1	1	L	G	L	L	G	G	G	G
	2	L	G	G	L	L	G	G	G
	3	L	G	G	G	L	L	G	G
	4	L	G	G	G	G	L	L	G
	5	L	G	G	G	G	G	L	L
	6	L	G	G	G	G	G	G	L
	7	L	L	G	G	G	G	G	G
	8	L	L	G	L	L	G	G	G
	9	L	L	G	G	L	L	G	G
	10	L	L	G	G	G	L	L	G
	11	L	L	G	G	G	G	L	L
	12	L	L	G	G	G	G	G	L
	13	L	G	L	G	L	G	L	G
	14	L	L	G	L	G	L	G	L
2	1	G	L	G	L	L	G	G	G
	2	G	L	G	G	L	L	G	G
	3	G	L	G	G	G	L	L	G
	4	G	L	G	G	G	G	L	L
	5	G	L	G	G	G	G	G	L
	6	G	L	L	G	G	G	G	G
	7	G	L	L	G	L	L	G	G
	8	G	L	L	G	G	L	L	G
	9	G	L	L	G	G	G	L	L
	10	G	L	L	G	G	G	G	L
	11	G	L	G	L	G	L	G	L
	12	G	L	L	G	L	G	L	G
3	1	G	G	L	G	L	L	G	G
	2	G	G	L	G	G	L	L	G
	3	G	G	L	G	G	G	L	L
	4	G	G	L	G	G	G	G	L
	5	G	G	L	L	G	G	G	G
	6	G	G	L	L	G	L	L	G
	7	G	G	L	L	G	G	L	L
	8	G	G	L	L	G	L	G	L
	9	G	G	L	G	L	G	L	G
4	1	G	G	G	L	G	L	L	G
	2	G	G	G	L	G	G	L	L
	3	G	G	G	L	G	G	G	L
	4	G	G	G	L	L	G	G	G
	5	G	G	G	L	L	G	L	L
	6	G	G	G	L	G	L	G	L
	7	G	G	G	L	L	G	L	G
5	1	G	G	G	G	L	G	L	L
	2	G	G	G	G	L	G	G	L
	3	G	G	G	G	L	L	G	G
	4	G	G	G	G	L	L	G	L
	5	G	G	G	G	L	G	L	G
6	1	G	G	G	G	G	L	L	G
	2	G	G	G	G	G	L	G	L
7	1	G	G	G	G	G	G	L	G
	2	G	G	G	G	G	G	L	L
8	1	G	G	G	G	G	G	G	L

angle remained (the maximum error was 0.18 [rad]) but the method improved the position accuracy of the head when the robot changed the body shape.

VII. CONCLUSION

This paper presented a shape control method for a passive wheeled snake robot that maintains head position and orientation. This method is based on the model in which kinematic redundancy is represented as both the SCP and null space, and avoids joint limit and self-collision by switching of the grounded/lifted status of the wheels. Though the model and the controlled variable are switched, the control input does not jump. Simulation and experiment demonstrated the effectiveness of the proposed method.

Future works will investigate avoidance of the deadlock depending on static stability, and will plan an appropriate target shape for various gait patterns.

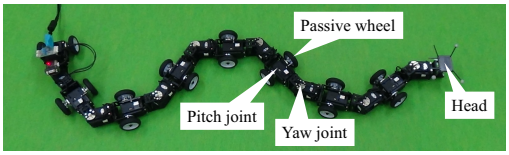

Fig. 6. Experimental snake robot.

(a) All joints rotate at the same time without considering kinematics.

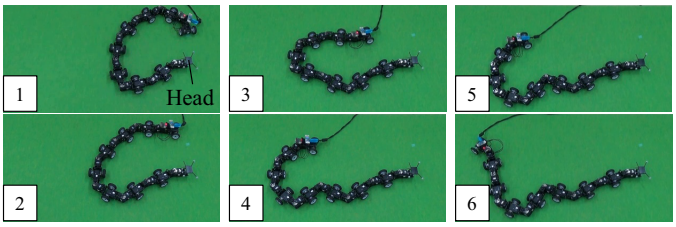

(b) Proposed method.

Fig. 7. Motion of the robot in the experiment.

ACKNOWLEDGMENTS

This work was partially supported by JSPS KAKENHI Grant Number 26870198, and the ImPACT Program of Council for Science, Technology and Innovation (Cabinet Office, Government of Japan).

REFERENCES

[1] P. Liljebäck, K. Y. Pettersen, Ø. Stavdahl, and J. T. Gravdahl, "A review on modelling, implementation, and control of snake robots," *Robotics and Autonomous Systems*, vol.60, pp.29-40, 2012.
[2] S. Hirose, Biologically Inspired Robots (Snake-like Locomotor and Manipulator), Oxford University Press, 1987.
[3] M. Nilsson, "Snake robot-free climbing," *IEEE Control System Magazine*, vol.18, no.1, pp.21-26, 1998.
[4] C. Ye, S. Ma, Y. Wang, and B. Li, "Coupled-Drive-Based Joint Design of a Snake Robot and its Body-Lifting Method," *Proc. IEEE Int. Conf. on Robotics, INtelligent Systems and Signal Processing*, pp.1086-1090, 2003.
[5] E. A. Cappo and H. Choset, "Planning End Effector Trajectories for a Serially Linked, Floating-base Robot with Changing Support Polygon," *Proc. American Control Conf.*, pp.4038-4043, 2014.
[6] M. Tanaka and F. Matsuno, "Modeling and Control of Head Raising Snake Robots by Using Kinematic Redundancy," *J. of Intelligent and Robotic Systems*, vol.75, no.1, pp.53-69, 2014.
[7] M. Tanaka and K. Tanaka, "Control of a Snake Robot for Ascending and Descending Steps," *IEEE Transactions on Robotics*, vol.31, no.2, pp.511-520, 2015.

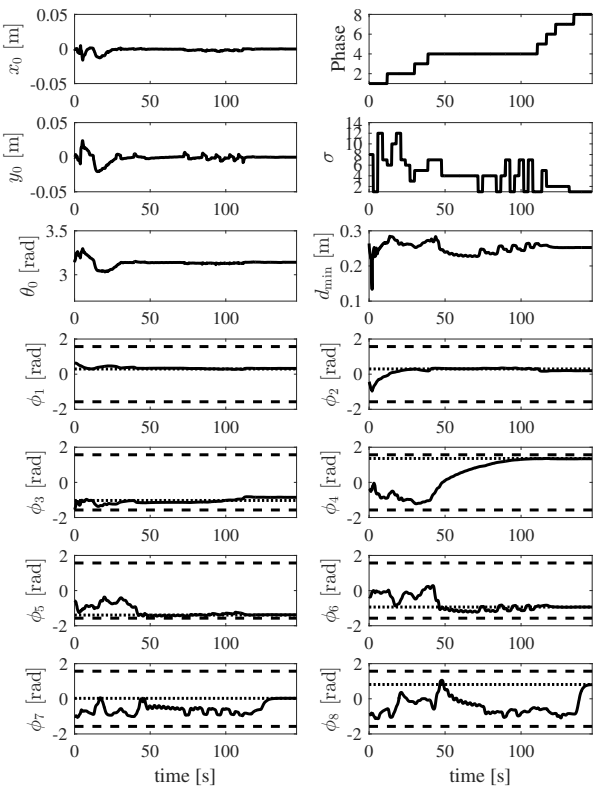

Fig. 8. Time responses of the experiment.

[8] K. Kon, M. Tanaka, and K. Tanaka, "Mixed Integer Programming Based Semi-autonomous Step Climbing of a Snake Robot Considering Sensing Strategy," *IEEE Transactions on Control Systems Technology*, vol.24, no.1, pp.252-264, 2016.

[9] K. Hoshino, M. Tanaka, and F. Matsuno, "Optimal Shape of a Snake Robot for Jumping," *Proc. IEEE Conf. on Robotics and Automations*, pp.697-702, 2010.

[10] M. Saito, M. Fukaya, and T. Iwasaki, "Serpentine Locomotion with Robotic Snakes," *IEEE Control Systems Magazine*, vol.22, no.1, pp.64-81, 2002.

[11] L. Zhu, Z. Chen, and T. Iwasaki, "Oscillation, Orientation, and Locomotion of Underactuated Multilink Mechanical Systems," *IEEE Trans. on Control Systems Technology*, vol.21, no.5, pp.1537-1548, 2013.

[12] P. Liljebäck, I. U. Haugstuen and K. Y. Pettersen, "Path Following Control of Planar Snake Robots Using a Cascaded Approach," *IEEE Trans. on Cont. Sys. Tech*, vol.20, no.1, pp.111-126, 2012.

[13] A. Mohammadi, E. Rezapour, M. Maggiore, and K. Y. Pettersen, "Maneuvering Control of Planar Snake Robots Using Vertual Holonomic Constraints," *IEEE Trans. on Control Systems Technology*, DOI: 10.1109/TCST.2015.2467208, early access articles.

[14] P. Prautsch, T. Mita, and T. Iwasaki, "Analysis and control of a gait of snake robot," *IEEJ Trans. on Industry Applications*, vol.120, no.3, pp.372-381, 2000.

[15] K. Watanabe, M. Iwase, S. Hatakeyama, and T. Maruyama, "Control Strategy for a Snake-Like Robot Based on Constraint Force and Verification by Experiment," *Advanced Robotics*, no.23, pp.907-937, 2009.

[16] M. Ishikawa, K. Owaki, M. Shinagawa, and T. Sugie, "Control of Snake-like Robot based on Nonlinear Controllability Analysis," *Proc. IEEE Int. Conf. on Control Applications*, pp.1134-1139, 2010.

[17] F. Matsuno and K. Mogi, "Redundancy Controllable System and Control of Snake Robot with Redundancy based on Kinematic Model", *Proc. IEEE Int. Conf. on Decision and Control*, pp. 4791-4796, 2000.

[18] H. Ponte, M. Queenan, C. Gong, C. Mertz, M. Travers, F. Enner, M. Hebert, and H. Choset, "Visual Sensing for Developing Autonomous Behavior in Snake Robots," *Proc. IEEE Int. Conf. on Robotics and Automation*, pp.2779-2784, 2014.

[19] P. Liljebäck, Ø. Stavdahl, K. Y. Pettersen, and J. T. Gravdahl, "Mamba - A Waterproof Snake Robot with Tactile Sensing," *IEEE/RSJ Int. Conf. on Intelligent Robots and Systems*, pp.294-301, 2014.

[20] K. Kouno, H. Yamada, and S. Hirose, "Development of Active-Joint Active-Wheel High Traversability Snake-Like Robot ACM-R4.2," *J. of Robotics and Mechatronics*, vol.25, no.3, pp.559-566, 2013.

[21] L. Pfotzer, M. Staehler, A. Hermann, A. Roennau, and R. Dillmann, "KAIRO 3: Moving Over Stairs & Unknown Obstacles with Reconfigurable Snake-Like Robots," *Proc. European Conf. on Mobile Robots*, pp.1-6, 2015.

[22] M. Tanaka, K. Kon, and K. Tanaka, "Range-sensor-based Semiautonomous Whole-body Collision Avoidance of a Snake Robot," *IEEE Trans. on Control Systems Technology*, vol.23, no.5, pp.1927-1934, 2015.

[23] M. Mutlu, K. Melo, M. Vespignani, A. Bernardino, and A. J. Ijspeert, "Where to Place Cameras on a Snake Robot: Focus on Camera Trajectory and Motion Blur," *Proc. 2015 IEEE Int. Symp. on Safety, Security, and Rescue Robotics*, pp.1-8, 2015.

[24] A. Transeth, R. Leine, C. Glocker, K. Pettersen, and P. Liljebäck, "Snake Robot Obstacle-Aided Locomotion: Modeling, Simulations, and Experiments," *IEEE Trans. on Robotics*, vol.24, no.1, pp.88-104, 2008.

[25] T. Kamegawa, R. Kuroki, and A. Gofuku, "Evaluation of Snake Robot's Behavior Using Randomized EARLI in Crowded Obstacles," *Proc. IEEE Int. Symp. on Safety, Security, and Rescue Robotics*, pp.1-6, 2014.

[26] X. Wu and S. Ma, "Neurally Controlled Steering for Collision-Free Behavior of a Snake Robot," *IEEE Trans. on Control Systems Technology*, vol.21, no.6, pp.2443-2449, 2013.

[27] D. Yagnik, J. Ren, and R. Liscano, "Motion Planning for Multi-Link Robots Using Artificial Potential Fields and Modified Simulated Annealing," *Proc. IEEE/ASME Int. Conf. on Mechatronics and Embedded Systems and Applications*, pp.421-427, 2010.

[28] Y. Hitaka and M. Yokomichi, "Obstacle Avoidance of a Snake Robot in Narrow Hallway," *Proc. IEEE Int. Conf. on Mechatronics and Automation*, pp.214-219, 2012.

[29] M. Tanaka, F. Matsuno, "Control of Snake Robots with Switching Constraints: trajectory tracking with moving obstacle," *Advanced Robotics*, vol.28, issue 6, pp.415-429, 2014.

[30] M. Tanaka, K. Tanaka, and F. Matsuno, "Approximate Path-Tracking Control of Snake Robot Joints with Switching Constraints," *IEEE/ASME Trans. on Mechatronics*, vol.20, no.4, pp.1633-1641, 2015.

[31] M. Tanaka and K. Tanaka, "Shape Control for a Snake Robot via Sequential Switching," *Proc. SWARM 2015: The First International Symposium on Swarm Behavior and Bio-Inspired Robotics*, P2-3, pp.200-202, 2015.

[32] M. Gienger, H. Janben, and C. Goerick, "Task-Oriented Whole Body Motion for Humanoid Robots," *Proc. 5th IEEE-RAS Int. Conf. on Humanoid Robots*, pp.238-244, 2005.

[33] M. Schwienbacher, T. Buschmann, S. Lohmeier, V. Favot, and H. Ulbrich, "Self-Collision Avoidance and Angular Momentum Compensation for a Biped Humanoid Robot," *Proc. IEEE Int. Conf. on Robotics and Automation*, pp.581-586, 2011.

[34] M. Tanaka, M. Nakajima, and K. Tanaka, "Smooth Control of an Articulated Mobile Robot with Switching Constraints," *Advanced Robotics*, vol.30, no.1, pp.31-40, 2016.

[35] S. Hirose, E. F. Fukushima, and S. Tsukagoshi, "Basic Steering Control Methods for The Articulated Body Mobile Robot," *IEEE Control Systems Magazine*, vol.15, no.1, pp.5-14, 1995.

[36] K. L. Paap, F. Kirchner, and B. Klaassen, "Motion Control Scheme for a Snake-Like Robot," *Proc. IEEE Int. Symp. on Computational Intelligence in Robotics and Automation*, pp.59-63, 1999.

[37] M. Kolesnik and H. Streich, "Visual Orientation and Motion Control of MAKRO–Adaptation to the Sewer Environment," *Proc. 7th Int. Conf. on Simulation of Adaptive Behavior on from animals to animats*, pp.62-69, 2002.

[38] H. Yamada and S. Hirose, "Development of Practical 3-Dimensional Active Cord Mechanism ACM-R4," *J. of Robotics and Mechatronics*, vol.18, no.3, pp.305-311, 2006.

[39] B. Murugendran, A. A. Transeth, and S. A. Fjerdingen, "Modeling and Path-following for a Snake Robot with Active Wheels," *IEEE/RSJ Int. Conf. on Intelligent Robots and Systems*, pp.3643-3649, 2009.

[40] C. Gong, M. Travers, H. C. Astley, D. I. Goldman, and H. Choset, "Limbless Locomotors that Turn in Place," *Proc. IEEE Int. Conf. on Robotics and Automation*, pp.3747-3754, 2015.